

Electrochemical sensor for nitrite using a glassy carbon electrode modified with gold-copper nanochain networks

Su-Su Huang¹ · Li Liu² · Li-Ping Mei¹ · Jia-Ying Zhou¹ · Fei-Ying Guo¹ ·
Ai-Jun Wang¹ · Jiu-Ju Feng¹

Received: 20 September 2015 / Accepted: 3 December 2015 / Published online: 28 December 2015
© Springer-Verlag Wien 2015

Abstract Bimetallic gold-copper nanochain networks (AuCu NCNs) were prepared by a single-step wet-chemical approach using metformin as a growth-directing agent. The formation mechanism was investigated in detail, and the AuCu NCNs were characterized by transmission electron microscopy (TEM), X-ray photoelectron spectroscopy (XPS) and X-ray diffraction (XRD). The nanocrystals were deposited on glassy carbon electrode and this resulted in a highly sensitive sensor for nitrite. Features include a low working potential (best at 0.684 V vs. SCE), fair sensitivity ($17.55 \mu\text{A mM}^{-1}$), a wide linear range (0.01 to 4.0 mM), a low detection limit (0.2 μM , S/N = 3), and superior selectivity as compared to other sensors.

Keywords Metformin · Bimetallic structures · Cyclic voltammetry · High-resolution TEM · Annular dark-field scanning TEM

Electronic supplementary material The online version of this article (doi:10.1007/s00604-015-1717-z) contains supplementary material, which is available to authorized users.

✉ Jiu-Ju Feng
jjfeng@zjnu.cn

¹ College of Chemistry and Life Science, College of Geography and Environmental Science, Zhejiang Normal University, Jinhua 321004, China

² Jinhua Agricultural Products Quality Comprehensive Supervision and Inspection Center, Yongkang St. 209, Jinhua 321017, China

Introduction

Nitrite (NO_2^-) has undesirable effects on both environmental protection and human health [1]. As a common food additive and preservative, nitrite is widely applied in industry and can be found in food and the environment [2]. It is also present in water by chlorination reactions inducing the formation of nitrite in water system [3]. According to the World Health Organization, the maximum limit of nitrite in drinking water is 3 mg L^{-1} [4]. Nitrite contamination in drinking water would cause different diseases, including “Blue Baby Syndrome”, methemoglobinemia, and stomach cancer caused by the formation of carcinogenic *N*-nitrosamines when it reacts with amine in stomach [5]. Thus, it is significant to develop a simple, rapid and sensitive method to determine nitrite for public health and environmental security [6].

Diverse detection techniques have been developed for the determination of nitrite, including spectrophotometry [7], fluorescence spectroscopy [8], and high performance liquid chromatography [9]. However, these methods are insensitive, time-consuming, and even toxicity by using toxic agents [4].

Electroanalysis has high sensitivity and selectivity, simplicity, and low cost [10]. Much work has been focused on developing a rapid electrochemical method for nitrite detection, without sample pretreatment and interference from other readily reducible compounds (such as nitrate ions and molecular oxygen).

Nanomaterial-based electrochemical nitrite sensors were fabricated to overcome the above limitations [11, 12]. Bimetallic nanostructures have been extensively investigated as electrode materials because of their good biocompatibility and conductivity, enlarged specific surface area, and enhanced catalytic activity [13]. Wang et al. have investigated the

electrochemical sensing activities of nanoporous palladium-iron alloy toward nitrite with the aim to construct a highly sensitive and stable electrochemical sensor [14].

Particularly, bimetallic Au-based alloys possess remarkable catalytic activity as compared with their mono-counterparts. Several examples (e.g., AuPt [15], AuPd [16], and AuCu [17] bimetallic alloys) demonstrate much higher catalytic activity relative to monometallic Au particles. Among them, AuCu alloys have attracted considerable attention for the construction of electrochemical sensors, owing to the relatively low cost and superior catalytic activity [18]. For example, Chen et al. fabricated a potential pH sensor based on AuCu nanoclusters with pH-dependent photoluminescence property [19]. In another example, Wang and co-workers constructed a highly sensitive H₂O₂ sensor based on AuCu nanowires [20].

Herein, gold-copper nanochain networks (AuCu NCNs) were rapidly fabricated by a simple one-step wet-chemical approach with the help of metformin, which was explored for the fabrication of a sensor by the detection of nitrite as a model system.

Experimental section

Chemicals

Copper chloride (CuCl₂), chloroauric acid (HAuCl₄), sodium borohydride (NaBH₄), metformin hydrochloride, ethanol and sodium nitrite were obtained from Shanghai Aladdin Chemical Reagent Company (Shanghai, China, www.chemicalbook.com). Other chemicals were of analytical grade. Twice-distilled water was employed throughout all the experiments.

Synthesis of AuCu NCNs

Typical preparation of AuCu NCNs was described as follows: Firstly, 0.041 g of metformin was dissolved into 8.0 mL of water, followed by mixing with 823 μ L of HAuCl₄ (24.3 mM) and 1.0 mL of CuCl₂ (20 mM) together in ice-bath (0 °C). After stirring for 10 min, 200 μ L of the freshly-prepared NaBH₄ solution (1.0 M) was drop-wise added to the mixed solution under stirring. Finally, the resulting black precipitates were separated by centrifugation, thoroughly washed with water and ethanol, and then dried at 60 °C. For comparison, control samples were also prepared with the Au/Cu molar ratio of 1:3 and 3:1 (defined as Au₁Cu₃ and Au₃Cu₁), respectively. And Au nanoparticles were synthesized according to the previous report [21].

Preparation of AuCu NCNs/GCE

To prepare AuCu NCNs modified electrode, 2.0 mg of the sample was dispersed into 1.0 mL of water under ultrasonication for 20 min. Subsequently, 6 μ L of the resulting suspension was dropped on the clean glassy carbon electrode (GCE, 3.0 mm in diameter) and allowed to dry in air. The resulting electrode was denoted as AuCu NCNs/GCE. And Au nanoparticles/GCE was prepared for comparison in a similar way. The details of instrumental characterization and electrochemical experiments were provided in the Electronic Supplementary Material.

Results and discussion

Characterization

Figure 1A and B show transmission electron microscopy (TEM) and high-resolution TEM (HR-TEM) images of the product. A lot of uniform nanochain networks are observed across the whole section. The nanochains are consisted of branched nanoparticles with an averaged diameter of 5.1 ± 0.2 nm as building units, which are assembled to form branched nanochains extending to hundreds of nanometers in length. As shown in Fig. S1 (Electronic Supplementary Material, ESM), the chain-like structure for AuCu products is well kept instead of a phase separation between Au and Cu atoms after two months, indicating long-term stability of the nanochains. And their polycrystalline nature is manifested by the selective area electron diffraction pattern (inset in the Fig. 1B).

Moreover, HR-TEM image (Fig. 1C) exhibits well-resolved lattice fringes with the inter-planar distance of 0.23 ± 0.002 nm, corresponding to the (111) planes of the face-centered cubic (fcc) AuCu alloy [22], indicating the predominant crystal growth along the direction of the (111) planes. This observation is identical with the previous study [23].

To analyze the elemental distribution in AuCu NCNs, high angle annular dark-field scanning TEM (HAADF-STEM) mapping images and cross-section compositional line profiles were supplied (Fig. 2). The resultant patterns exhibit uniform distribution of Au and Cu elements in AuCu NCNs, strongly verifying the formation of AuCu alloy [24].

The crystalline nature of AuCu NCNs was investigated by X-ray diffraction (XRD, Fig. 3). There are five characteristic peaks emerged at around 38.5°, 44.5°, 65.1°, 77.8°, and 82.3°, which are assigned to the (111), (200), (220), (311) and (222) planes of AuCu NCNs [25], respectively. The diffraction peaks are slightly shifted and lie between pure Au (JCPDS-04-0784) and Cu (JCPDS-04-0836), indicating the formation of AuCu alloy [26]. In addition, the peaks detected at 35.5°

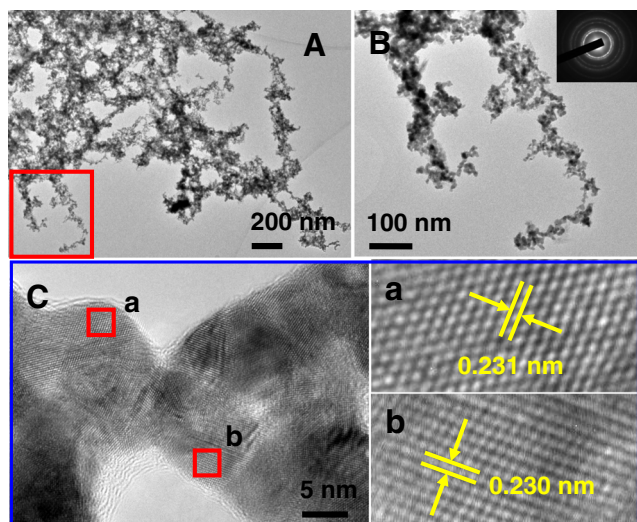


Fig. 1 TEM (A and B) and HR-TEM (C) images of AuCu NCNs. *Inset* in B shows the corresponding SAED pattern

and 48.8° might be originated from CuO, owing to the incomplete reduction of CuCl_2 or surface Cu oxidation under ambient conditions [27].

The oxidation state and surface composition of AuCu NCNs were surveyed by XPS (Fig. 4). The two prominent peaks observed at 83.82 and 87.51 eV are indexed to $4f_{7/2}$ and $4f_{5/2}$ feature of Au^0 (Fig. 4a) [28], respectively. Nevertheless, there is no obvious peak of Au^{3+} appeared, revealing the complete reduction of AuCl_4^- . As illustrated in Fig. 4b, two characteristic peaks emerge at around 932.3 and 952.2 eV corresponding to the binding energies of $2p_{1/2}$ and $2p_{3/2}$ of Cu^0 [29]. A shake-up is observed at 943 eV, confirming the existence of very minimal Cu^{2+} in AuCu NCNs generated from unreacted CuCl_2 [30]. Additionally, it's highly significant to mention that the $2p_{3/2}$ binding energy

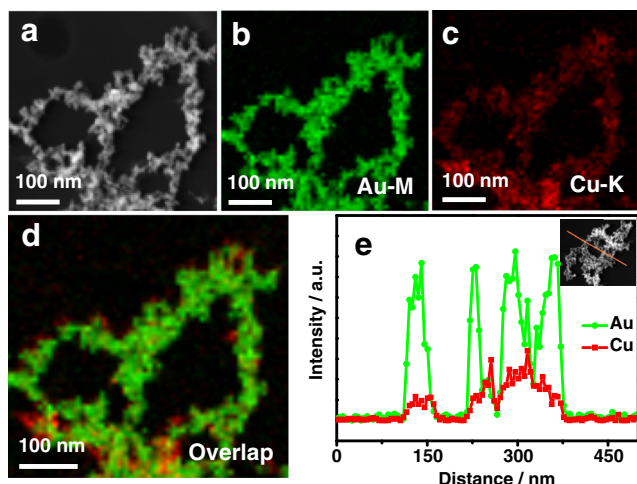


Fig. 2 HAADF-STEM-EDS mapping images (a–d), and cross-sectional compositional line profiles (e) of AuCu NCNs. *Inset* in e shows the corresponding HAADF-STEM image

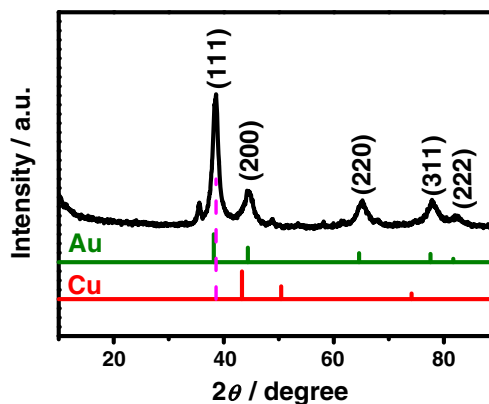


Fig. 3 XRD pattern of AuCu NCNs. The standard patterns of bulk Au (JCPDS-04-0784) and Cu (JCPDS-04-0836) are provided for comparison

of Cu^0 is only ~ 0.1 eV different from Cu^+ . Thus, the valence states of Cu herein may lie between 0 and +1 [31].

Formation mechanism

To better understand the formation mechanism of AuCu NCNs, a series of control experiments were carried out, including the metformin concentrations, the type of the reducing agent, and the molar ratio of Au/Cu. As shown in Fig. S2 (ESM), the absence of metformin yields a great deal of irregular nanoparticles with seriously aggregation (Fig. S2A, ESM). This is attributed to the formation of bare crystal planes without any capping agent to prevent them from aggregation [32]. The presence of 10 mM metformin produces chain-like nanocrystals with poor quality (Fig. S2B, ESM), and the best ones are produced with 25 mM metformin (Fig. 1). However, further increasing the concentration of metformin inhibits the chain length growth, causing the formation of short chains with aggregation (e.g., 50 mM, Fig. S2C, ESM). These results demonstrate metformin as a growth-directing agent and a weak stabilizing agent in the present synthesis [33].

Similarly, different reducing agent was also found to be essential in controlling the morphology of AuCu alloy nanocrystals. When ascorbic acid is used, the

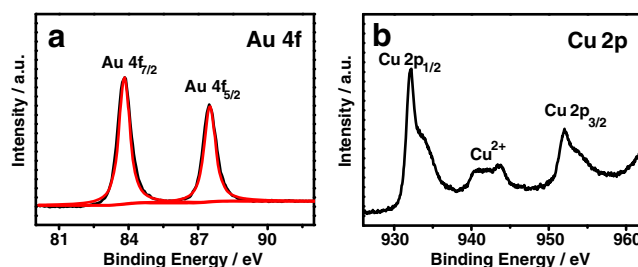


Fig. 4 High-resolution XPS spectra of Au 4f (a) and Cu 2p (b) in AuCu NCNs

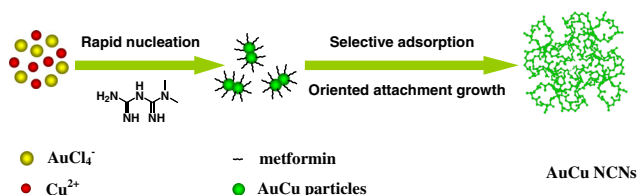


Fig. 5 Schematic illustration of the formation mechanism of AuCu NCNs

product contains severely aggregated AuCu nanoparticles with broad size distribution, rather than AuCu NCNs (Fig. S3A, ESM). By reducing the precursors with hydrazine hydrate (Fig. S3B, ESM), the product contains many poor nanochain networks. These results apparently demonstrate that the morphology of the product can be well controlled by the reaction kinetics [34]. Moreover, the Au/Cu molar ratio was also confirmed to be a main factor in shaping the final products, as displayed in Fig. S4 (ESM). When the Au/Cu molar ratio is 1:3 (Fig. S4A, ESM), only some irregular and agglomerated AuCu nanoparticles are obtained, while aggregated nanochains are observed with the Au/Cu molar ratio of 3:1 (Fig. S4B, ESM). It reveals that the Au/Cu molar ratio of the two precursors is strongly related to the nucleation and growth kinetics, therefore affecting the final morphology of the products [26].

The formation mechanism of AuCu NCNs can be described by a three-step growth model: rapid nucleation, selective adsorption, and oriented attachment growth. As shown in Fig. 5, numerous Au and Cu atoms are rapidly generated upon the addition of NaBH_4 at the very early stage, owing to the extremely strong reducing ability of NaBH_4 [35]. Immediately, the newly-formed Au and Cu atoms transform to AuCu nuclei, which are selectively adsorbed by metformin molecules on the (100) and (110) crystal planes with lower energies, facilitating the predominant

growth along the (111) directions [19, 36, 37], as strongly confirmed by the associated HR-TEM images (Fig. 1C). Finally, AuCu NCNs are formed with the electrostatic interactions and oriented attachment with the assistance of metformin.

Electrocatalytic oxidation of nitrite at AuCu NCNs/GCE

The electrocatalytic behaviors of AuCu NCNs/GCE (curve a), Au nanoparticles/GCE (curve b), GCE (curve c), Au_1Cu_3 nanoparticles/GCE (curve d), and Au_3Cu_1 nanoparticles/GCE (curve e) were studied by cyclic voltammetry (CV) in 1.0 mM nitrite (Fig. 6A). Apparently, the oxidation peak current of nitrite for AuCu NCNs/GCE ($40.33 \pm 0.012 \mu\text{A}$, at 0.851 V vs. SCE) is about 1.54 ± 0.01 , 1.68 ± 0.017 , 6.06 ± 0.02 , and 6.50 ± 0.019 times larger than those at bare GCE ($26.13 \pm 0.02 \mu\text{A}$, at 1.081 V vs. SCE) and Au nanoparticles/GCE ($23.94 \pm 0.027 \mu\text{A}$, at 0.788 V vs. SCE), Au_1Cu_3 nanoparticles/GCE ($6.655 \pm 0.021 \mu\text{A}$, at 0.834 V vs. SCE), and Au_3Cu_1 nanoparticles/GCE ($6.208 \pm 0.017 \mu\text{A}$, at 0.818 V vs. SCE), respectively. Besides, the anodic peak for AuCu NCNs/GCE at 0.207 V is attributed to the conversion of Cu(0)–Cu(I) [38]. The cathodic peaks at 0.155 V and 0.419 V are attributed to the transition of Cu(II) to Cu(I) and of Cu(I) to Cu(0), respectively [39]. The improved peak current and more negative peak potential is ascribed to the enhanced specific surface area of AuCu NCNs, high conductivity, and synergistic effects between Au and Cu in AuCu NCNs.

The electrocatalytic behaviors of AuCu NCNs/GCE were examined in 1.0 mM nitrite at various scan rates (Fig. 6B). It is observed that the oxidation peak currents increase gradually with the scan rates ($10 \sim 100 \text{ mV s}^{-1}$), accompanied with the positive shift of the peak potentials. However, the oxidation peak current of nitrite is in proportion to the square root of scan rate with a correlation coefficient (R^2) of 0.9988 (inset in Fig. 6B), which

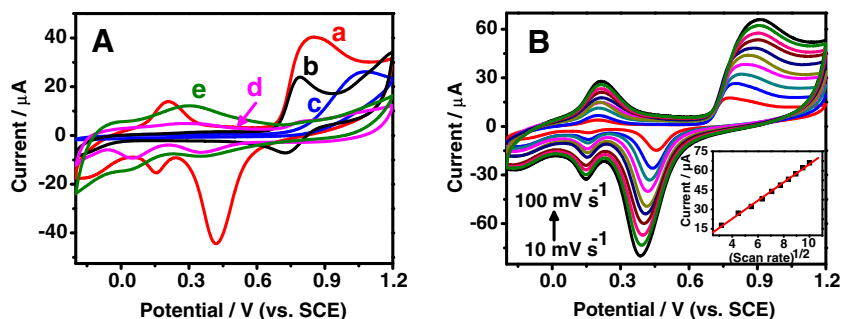


Fig. 6 **A** Cyclic voltammograms of 1.0 mM nitrite on AuCu NCNs/GCE (curve a), Au nanoparticles/GCE (curve b), and bare GCE (curve c) in 0.1 M phosphate buffer (pH 7.0) at a scan rate of 50 mV s^{-1} . **(B)** Cyclic voltammograms of AuCu NCNs/GCE in 0.1 M phosphate buffer (pH 7.0)

containing 1.0 mM nitrite at different scan rates from 10 to 100 mV s^{-1} . Inset shows the linear relationship between the oxidation peak current of nitrite and the square root of scan rate at 0.78 V (vs. SCE)

exhibits the diffusion-controlled process in the determination of nitrite [40].

Fig. S5 (ESM) shows the effects of pH values on the electrocatalytic behavior toward 1.0 mM nitrite oxidation at AuCu NCNs/GCE by varying the pH values from 3.0 to 9.0. The peak current achieves the maximum at pH 7.0 and then decreases by further extending the pH values. This is attributed to the fact that nitrite is instable in acidic media [41] and the nitrite oxidation becomes more difficulty with the lack of protons in alkaline media [42]. Therefore, pH 7.0 was employed in the subsequent experiments.

Figure 7 displays the oxidation peak currents from the differential pulse voltammetry with various nitrite concentrations at AuCu NCNs/GCE under the optimized conditions. Clearly, the peak current is proportional to the nitrite concentration with the linear range of 0.01 ~ 4.0 mM. The linear calibration equation was I_p (μA) = 0.0176 C (μM) - 0.0176 (correlation coefficient, $R^2 = 0.9994$). The sensitivity is 0.0176 $\mu\text{A } \mu\text{M}^{-1}$ with the limit of detection (LOD) of 0.2 μM ($S/N = 3$). Clearly, the presence of AuCu NCNs improves the catalytic performance for nitrite sensing in terms of sensitivity and LOD as compared to those in previous reports (Table 1) [2, 40, 43–45].

The reproducibility and stability of AuCu NCNs/GCE were determined in 1.0 mM nitrite. The fabrication reproducibility for five electrodes prepared independently was calculated by the responses to 1.0 mM nitrite with the relative standard deviation (RSD) of 1.7 %. Moreover, the RSD of current responses with the same electrode was 1.9 % for five successive measurements. These results suggest good reproducibility of this approach. After storing in refrigerator at 4 °C for 35 days, the peak current responses were still retained 98.60 % of the initial values on AuCu NCNs/GCE, revealing good stability of the sensor for the detection of nitrite.

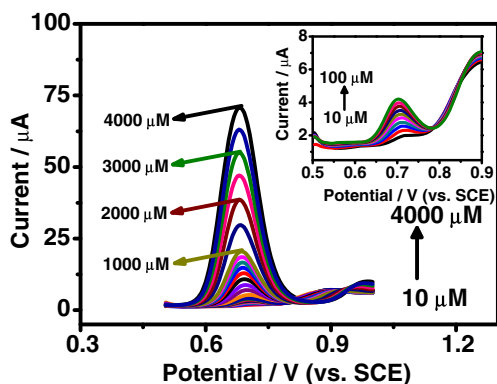


Fig. 7 Differential pulse voltammetry curves of AuCu NCNs/GCE in the presence of different nitrite concentrations at 0.68 V (vs. SCE)

Table 1 Comparison of this sensor for nitrite determination with those in the literature

Modified materials	Linear range (μM)	Detection limit (μM)	Ref.
Gold nanoparticles/choline chloride/GCE	0.4–750	0.1	[2]
Cobalt nitroprusside/GCE	20–22,000	10	[40]
Gold nanoparticles/sulfonated graphene	10–3960	0.2	[43]
multi-walled carbon nanotubes	0.5–250	0.3	[44]
Didodecyltrimethylammonium bromide/GCE	1.0–80	-	[45]
AuCu NCN	10–4000	0.2	This work

The excellent long-term stability and reproducibility of AuCu NCNs/GCE make them attractive in the field of analytical applications.

The selectivity was studied by adding some potentially interfering ions to the phosphate buffer (pH 7.0) containing 0.5 mM nitrite. It is found that 100 folds of NaCl, CH_3COONa , NaNO_3 , NaCO_3 , NaSO_4 , and CH_3OH have no interference on nitrite determination, as shown in Fig. S6 (ESM). These results reveal this sensor has high selectivity for nitrite, which is attributed to the strong affinity between nitrite and metallic nanocrystals [46].

To evaluate the feasibility of nitrite detection in real samples, AuCu NCNs/GCE was employed to determine nitrite in water samples. As listed in Table S1 (ESM), the recoveries ranged from 99.8 % to 103.4 % for five parallel measurements, with RSD below 4.1 %. Therefore, AuCu NCNs/GCE can be utilized to determine nitrite in real water samples.

Conclusion

In summary, AuCu NCNs were successfully prepared and employed for the construction of a highly selective electrochemical sensor for the detection of nitrite. This sensor exhibited significantly enhanced catalytic performance toward nitrite oxidation as compared with the referenced sensors. The wide linear range, high selectivity, good stability, low detection limit and high reproducibility make it a potential candidate for practical applications.

Acknowledgments This work was financially supported by National Natural Science Foundation of China (No. 21475118, 21175118 and 21275130) and Zhejiang province of undergraduate scientific and technological innovation project (New Talents Program, No. 2015404004 for S.S. Huang).

References

- Yang S, Xia B, Zeng X, Luo S, Wei W, Liu X (2010) Fabrication of DNA functionalized carbon nanotubes/Cu²⁺ complex by one-step electrodeposition and its sensitive determination of nitrite. *Anal Chim Acta* 667:57
- Wang P, Mai Z, Dai Z, Li Y, Zou X (2009) Construction of Au nanoparticles on choline chloride modified glassy carbon electrode for sensitive detection of nitrite. *Biosens Bioelectron* 24:3242
- Afkhami A, Soltani-Felehgari F, Madrakian T, Ghaedi H (2014) Surface decoration of multi-walled carbon nanotubes modified carbon paste electrode with gold nanoparticles for electro-oxidation and sensitive determination of nitrite. *Biosens Bioelectron* 51:379
- Radhakrishnan S, Krishnamoorthy K, Sekar C, Wilson J, Kim SJ (2014) A highly sensitive electrochemical sensor for nitrite detection based on Fe₂O₃ nanoparticles decorated reduced graphene oxide nanosheets. *Appl Catal B* 148–149:22
- Mirvish SS (1995) Role of N-nitroso compounds (NOC) and N-nitrosation in etiology of gastric, esophageal, nasopharyngeal and bladder cancer and contribution to cancer of known exposures to NOC. *Cancer Lett* 93:17
- Zhou L, Wang J-P, Gai L, Li D-J, Li Y-B (2013) An amperometric sensor based on ionic liquid and carbon nanotube modified composite electrode for the determination of nitrite in milk. *Sensors Actuators B Chem* 181:65
- Aydin A, Ercan Ö, Taşcıoğlu S (2005) A novel method for the spectrophotometric determination of nitrite in water. *Talanta* 66:1181
- Liu H, Yang G, Abdel-Halim E, Zhu J-J (2013) Highly selective and ultrasensitive detection of nitrite based on fluorescent gold nanoclusters. *Talanta* 104:135
- Ito K, Takayama Y, Makabe N, Mitsui R, Hirokawa T (2005) Ion chromatography for determination of nitrite and nitrate in seawater using monolithic ODS columns. *J Chromatogr A* 1083:63
- Sudarvizhi A, Siddiqha ZA, Pandian K (2014) Single step synthesis of graphene oxide protected silver nanoparticles using aniline as reducing agent and study its application on electrocatalytic detection of nitrite in food samples. *J Chem Applied Biochem* 1:101
- Salimi A, Kurd M, Teymourian H, Hallaj R (2014) Highly sensitive electrocatalytic detection of nitrite based on SiC nanoparticles/amine terminated ionic liquid modified glassy carbon electrode integrated with flow injection analysis. *Sensors Actuators B Chem* 205:136
- Marlinda A, Pandikumar A, Yusoff N, Huang N, Lim H (2015) Electrochemical sensing of nitrite using a glassy carbon electrode modified with reduced functionalized graphene oxide decorated with flower-like zinc oxide. *Microchim Acta* 182:1113
- Chen K-J, Chandrasekara Pillai K, Rick J, Pan C-J, Wang S-H, Liu C-C, Hwang B-J (2012) Bimetallic PtM (M = Pd, Ir) nanoparticle decorated multi-walled carbon nanotube enzyme-free, mediator-less amperometric sensor for H₂O₂. *Biosens Bioelectron* 33:120
- Wang J, Zhou H, Fan D, Zhao D, Xu C (2015) A glassy carbon electrode modified with nanoporous PdFe alloy for highly sensitive continuous determination of nitrite. *Microchim Acta* 182:1055
- Dao V-D, Choi Y, Yong K, Larina LL, Shevaleevskiy O, Choi H-S (2015) A facile synthesis of bimetallic AuPt nanoparticles as a new transparent counter electrode for quantum-dot-sensitized solar cells. *J Power Sources* 274:831
- Garcia T, Murillo R, Agouram S, Dejoz A, Lazaro MJ, Torrente-Murciano L, Solsona B (2012) Highly dispersed encapsulated AuPd nanoparticles on ordered mesoporous carbons for the direct synthesis of H₂O₂ from molecular oxygen and hydrogen. *Chem Commun* 48:5316
- Wang G, Xiao L, Huang B, Ren Z, Tang X, Zhuang L, Lu J (2012) AuCu intermetallic nanoparticles: surfactant-free synthesis and novel electrochemistry. *J Mater Chem* 22:15769
- Xu Z, Lai E, Shao-Horn Y, Hamad-Schifferli K (2012) Compositional dependence of the stability of AuCu alloy nanoparticles. *Chem Commun* 48:5626
- Shibu Joseph ST, Ipe BI, Pramod P, Thomas KG (2006) Gold nanorods to nanochains: Mechanistic investigations on their longitudinal assembly using α, ω -alkanedithiols and interplasmon coupling. *J Phys Chem B* 110:150
- Wang N, Han Y, Xu Y, Gao C, Cao X (2015) Detection of H₂O₂ at the nanomolar level by electrode modified with ultrathin AuCu nanowires. *Anal Chem* 87:457
- Dang Y-Q, Li H-W, Wang B, Li L, Wu Y (2009) Selective detection of trace Cr³⁺ in aqueous solution by using 5,5'-dithiobis (2-nitrobenzoic acid)-modified gold nanoparticles. *ACS Appl Mater Inter* 1:1533
- Khanal S, Bhattarai N, McMaster D, Bahena D, Velazquez-Salazar JJ, Jose-Yacamán M (2014) Highly monodisperse multiple twinned AuCu-Pt trimetallic nanoparticles with high index surfaces. *Phys Chem Chem Phys* 16:16278
- Ding X, Zou Y, Jiang J (2012) Au–Cu₂S heterodimer formation via oxidation of AuCu alloy nanoparticles and in situ formed copper thiolate. *J Mater Chem* 22:23169
- Wi J-S, Tominaka S, Uosaki K, Nagao T (2012) Porous gold nanodisks with multiple internal hot spots. *Phys Chem Chem Phys* 14:9131
- Jiang Z, Zhang Q, Zong C, Liu B-J, Ren B, Xie Z, Zheng L (2012) Cu–Au alloy nanotubes with five-fold twinned structure and their application in surface-enhanced raman scattering. *J Mater Chem* 22:18192
- He R, Wang Y-C, Wang X, Wang Z, Liu G, Zhou W, Wen L, Li Q, Wang X, Chen X (2014) Facile synthesis of pentacle gold–copper alloy nanocrystals and their plasmonic and catalytic properties. *Nat Commun* 5:4327
- Luo M-F, Fang P, He M, Xie Y-L (2005) In situ XRD, raman, and TPR studies of CuO/Al₂O₃ catalysts for CO oxidation. *J Mol Catal A Chem* 239:243
- Li X-R, Li X-L, Xu M-C, Xu J-J, Chen H-Y (2014) Gold nanodendrites on graphene oxide nanosheets for oxygen reduction reaction. *J Mater Chem A* 2:1697
- Goswami N, Giri A, Bootharaju M, Xavier PL, Pradeep T, Pal SK (2011) Copper quantum clusters in protein matrix: potential sensor of Pb²⁺ ion. *Anal Chem* 83:9676
- Wang W, Leng F, Zhan L, Chang Y, Yang XX, Lan J, Huang CZ (2014) One-step prepared fluorescent copper nanoclusters for reversible pH-sensing. *Analyst* 139:2990
- Wei W, Lu Y, Chen W, Chen S (2011) One-pot synthesis, photoluminescence, and electrocatalytic properties of subnanometer-sized copper clusters. *J Am Chem Soc* 133:2060
- Fang J, Chandrasekharan P, Liu X-L, Yang Y, Lv Y-B, Yang C-T, Ding J (2014) Manipulating the surface coating of ultra-small Gd₂O₃ nanoparticles for improved T1-weighted MR imaging. *Biomaterials* 35:1636
- Zhang Q-L, Ju K-J, Huang X-Y, Wang A-J, Wei J, Feng J-J (2015) Metformin mediated facile synthesis of AuPt alloyed nanochains with enhanced electrocatalytic properties for alcohol oxidation. *Electrochim Acta* 182:305
- Fu G, Wu K, Lin J, Tang Y, Chen Y, Zhou Y, Lu T (2013) One-pot water-based synthesis of Pt–Pd alloy nanoflowers and their superior electrocatalytic activity for the oxygen reduction reaction and remarkable methanol-tolerant ability in acid media. *J Phys Chem C* 117:9826
- Zhao L, Jiang D, Cai Y, Ji X, Xie R, Yang W (2012) Tuning the size of gold nanoparticles in the citrate reduction by chloride ions. *Nanoscale* 4:5071
- Tao AR, Habas S, Yang P (2008) Shape control of colloidal metal nanocrystals. *small* 4:310

37. Wang H, Dong Z, Na C (2013) Hierarchical carbon nanotube membrane-supported gold nanoparticles for rapid catalytic reduction of p-nitrophenol. *ACS Sustain Chem Eng* 1:746
38. Yang S, Zeng X, Liu X, Wei W, Luo S, Liu Y, Liu Y (2010) Electrocatalytic reduction and sensitive determination of nitrite at nano-copper coated multi-walled carbon nanotubes modified glassy carbon electrode. *J Electroanal Chem* 639:181
39. Biniak S, Pakuła M, Szymański GS, Świątkowski A (1999) Effect of activated carbon surface oxygen- and/or nitrogen-containing groups on adsorption of copper(ii) ions from aqueous solution. *Langmuir* 15:6117
40. Sabzi R (2007) Amperometric detection of nitrite on glassy carbon electrode modified with cobalt nitroprusside. *Port Electrochim Acta* 25:383
41. Brylev O, Sarrazin M, Roué L, Bélanger D (2007) Nitrate and nitrite electrocatalytic reduction on Rh-modified pyrolytic graphite electrodes. *Electrochim Acta* 52:6237
42. Huang X, Li Y, Chen Y, Wang L (2008) Electrochemical determination of nitrite and iodate by use of gold nanoparticles/poly (3-methylthiophene) composites coated glassy carbon electrode. *Sensors Actuators B Chem* 134:780
43. Li S-J, Zhao G-Y, Zhang R-X, Hou Y-L, Liu L, Pang H (2013) A sensitive and selective nitrite sensor based on a glassy carbon electrode modified with gold nanoparticles and sulfonated graphene. *Microchim Acta* 180:821
44. Meng Z, Liu B, Zheng J, Sheng Q, Zhang H (2011) Electrodeposition of cobalt oxide nanoparticles on carbon nanotubes, and their electrocatalytic properties for nitrite electrooxidation. *Microchim Acta* 175:251
45. Zhang Y, Luo L, Ding Y, Li L (2009) Electrochemical determination of nitrite in water samples using a glassy carbon electrode modified with didodecyldimethylammonium bromide. *Microchim Acta* 167:123
46. Li Y-F, Lv J-J, Zhang M, Feng J-J, Li F-F, Wang A-J (2015) A simple and controlled electrochemical deposition route to urchin-like Pd nanoparticles with enhanced electrocatalytic properties. *J Electroanal Chem* 738:1